NJC

ROYAL SOCIETY OF CHEMISTRY

PAPER

View Article Online
View Journal | View Issue

Cite this: *New J. Chem.*, 2023, **47**, 13286

Investigation of uranium oxide hydrates with barium(II) ions: structural diversity, uranium valences and implications†

Kimbal T. Lu,[ab] Yingjie Zhang, *[a] Tao Wei,[a] Timothy A. Ablott,[a] Jakub Plášil,[c] Inna Karatchevtseva[a] and Rongkun Zheng[b]

Received 21st March 2023,
Accepted 7th June 2023

DOI: 10.1039/d3nj01334k

rsc.li/njc

Although barium(II) ions play an important role in the natural weathering of the mineral uraninite (UO_{2+x}) and are expected to therefore do the same for spent nuclear fuel in geological disposal, the detailed structural understanding of this role is rather limited. In this work, we report the synthesis and characterisation of two new uranium oxide hydrate (UOH) phases with barium(II) ions, a layer-structured **UOH-Ba1** constructed with undulating uranyl oxide hydroxide layers incorporating hydrated interlayer barium(II) ions; and **UOH-Ba2** forming a complex three-dimensional structure by linking six different types of uranium polyhedrons with barium(II) ions located in the narrow channels. Both crystal structures were revealed using synchrotron single crystal X-ray diffraction and confirmed with powder X-ray or electron diffractions. While vibrational modes were elucidated by Raman, electronic structures and the presence of pentavalent uranium were investigated using diffuse reflectance spectroscopy. This work has provided insights into the complexity of uranium crystal chemistry in the presence of barium(II) ions and has implications to both uranium geochemistry in terms of the natural weathering of uraninite and the disposal of spent nuclear fuel in the underground repository.

1. Introduction

Uranium minerals and synthetic compounds have been extensively studied, owing to the revived interest in nuclear energy to mitigate the effects of climate change.[1] The in-depth understanding of uranium geochemistry and structural chemistry is directly relevant to the current uranium-based nuclear fuel cycle.[2] The uranium oxide mineral uraninite (UO_{2+x}: x = 0–0.25)[3] has been used as the natural analogue for the study of spent nuclear fuel (SNF) as the SNF discharged from the nuclear reactor, usually in the form of UO_2, is highly radioactive and poses significant risks to the general public.[4] As one of the candidate solutions, the direct long-term disposal of this SNF in the geologically stable underground repository is the most attractive SNF management strategy for countries where SNF reprocessing facilities are not available.[5–7] As an international pioneer, Finland is on schedule to operate the world first underground repository for SNF in 2024.[8] However, there are still concerns on the possible interactions of SNF including fission products and radionuclides from the decay process with the surrounding materials in the presence of underground water.[9] While the geological repositories are designed to have a reducing environment where SNF will remain stable, a possible accident could occur where underground water may be in contact with SNF during the long-term storage, leading to the alteration of SNF.[10] A 10-year long drip-test conducted in the 1990s has confirmed that SNF undergoes the same oxidation–hydration alteration pattern to that of uraninite.[11]

Comparable to the natural weathering of uraninite, the alteration of SNF can be viewed as an oxidation–hydration process where tetravalent U^{4+} is progressively converted to hexavalent U^{6+}. The U^{6+} is prominently present as uranyl ions $(UO_2)^{2+}$,[12,13] which are further bonded with O/OH ligands in the equatorial planes to form tetragonal, pentagonal, and hexagonal uranium polyhedra. These uranyl moieties then link together *via* edge- or corner-sharing to form uranyl oxide hydroxide layers which will incorporate either water molecules (if the layers are charge neutral) or interlayer cations from the nearby environment to form uranium oxide hydrate (UOH) phases/compounds.[14,15] So far there are more than two dozen UOH minerals incorporating monovalent (alkali),[16,17] divalent

[a] *Australian Nuclear Science and Technology Organisation, Locked Bag 2001, Kirrawee DC, NSW 2232, Australia. E-mail: yzx@ansto.gov.au*
[b] *School of Physics and Advanced Materials, University of Sydney, Ultimo, New South Wales 2007, Australia*
[c] *Institute of Physics ASCR, v.v.i., Na Slovance 2, 18221, Praha 8, Czech Republic*

† Electronic supplementary information (ESI) available: Powder XRD, SEM-EDS, supporting tables, check CIFs (PDF), crystallographic information files (CIFs), CSD-2247026 (**UOH-Ba1**) and 2247027 (**UOH-Ba2**). CCDC 2247026 and 2247027. For ESI and crystallographic data in CIF or other electronic format see DOI: **https://doi.org/10.1039/d3nj01334k**

(alkaline earth, transition metals and p-block metals),[18–20] or a combination of mono- and divalent metal ions[21] as interlayer cations for charge compensation. They differ mainly in the secondary metal ions and the O/OH ratios largely dependent on the fluid chemical composition and pH.[14] In addition, the uranyl oxide hydroxide layer topologies for various UOH minerals have been comprehensively reviewed.[22]

Hydrothermal synthesis in the laboratory has been used to assist the formation of the UOH compounds in a simulated natural environment. To date, more than two dozen of synthetic UOH compounds have been made with interlayer cations including alkali,[23,24] alkaline earth,[25,26] lead,[27] limited 3d transition metal[28–30] and lanthanide ions.[31–34] Complicating these UOH systems are a further number of compounds which have a slightly different structure where the apical oxygen of the uranyl ions on the layer shares the equatorial oxygen with an interlayer uranyl ion acting as a pillar, resulting in an open three-dimensional (3D) framework structure typically incorporating various cations in the framework channels. Synthetic compounds of this type of structure, with various cations such as $(NH_4)^+$,[35] Sr^{2+},[36] Y^{3+} and Tb^{3+},[37] Eu^{3+}, Gd^{3+},[38] Sm^{3+},[39] and U^{4+}[40] ions have been synthesised and extensively studied, highlighting the complexity and flexibility of the UOH systems. Furthermore, other types of 3D structures with Cs^{+}[36] and Pb^{2+}[27] are also being revealed.

In examining the SNF environment, barium is anticipated to play an important role during the early alteration of SNF due to its abundance in rocks and groundwater (0.0425% in the Earth crust),[41] and more importantly being a fission product from the nuclear fission of 235-uranium (up to 2% in the SNF depending on the fuel burn up).[42] Several uranyl minerals containing barium exist in nature including protasite $(Ba[(UO_2)_3O_3(OH)_2](H_2O)_3)$,[43] billietite $(Ba[(UO_2)_3O_2(OH)_3]_2(H_2O)_4)$,[44] bauranoite $(Ba[(UO_2)(O,OH)](H_2O)_{4.5})$,[45] and in trace amount as in calciouranoite $[(Ca, Ba, Pb)U_2O_7{\cdot}5(H_2O)]$,[46] meta-calciouranoite $[(Ca, Na, Ba)U_2O_7{\cdot}2H_2O]$,[46] and wölsendorfite $[(Pb, Ca, Ba)U_2O_7{\cdot}2H_2O]$.[47] With these minerals making up a reasonable percentage of the UOH minerals in the early stage of the alterations of uraninite, this appears to confirm that barium is likely to be involved in the alteration pathways of SNF. Detailed study of protasite and billietite have found that both minerals form layered UOH structures stabilised by the interlayer barium cations. However, protasite has an α-U_3O_8 type uranyl layer structure whilst billietite adopts both the α-U_3O_8 and β-U_3O_8 uranyl layer structures (Fig. 1), suggesting geological factors influence the preferred formation of one structure type over the other. Limiting the understanding of these factors is the scarcity of structural information, with the crystal structure of bauranoite unknown.[45] Interestingly, the significant difference in the charge deficiency per anion (CDA) value between protasite and billietite, a value being used to measure the degree of oxidative alteration with a higher value indicating a later stage of alteration, suggests the possible existence of unexplored intermediate phases that could elucidate the factors governing the transition from β-U_3O_8 to α-U_3O_8 type uranyl oxide hydroxide layer in **UOH-Ba** system. With the difficulties in finding the suitable single crystal in nature and the limited number of minerals of which to study, hindering this progress, the recent success in the hydrothermal synthesis of UOH compounds can ideally overcome this challenge.[34]

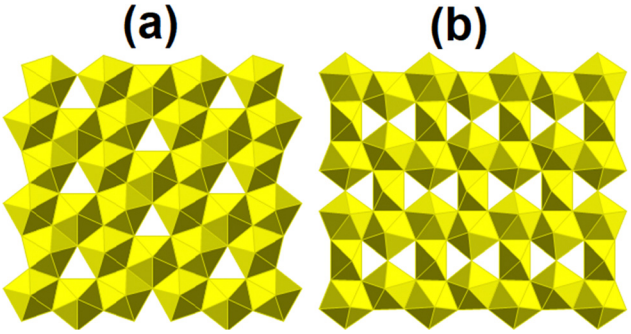

Fig. 1 Polyhedral views of uranyl oxide hydroxide layers: α-U_3O_8 type (a) and β-U_3O_8 type (b).

There is only one reported synthetic **UOH-Ba** phase, made *via* a hydrothermal reaction of schoepite and barium nitrate at 200 °C for 10 h. The compound was characterised using X-ray diffraction and IR but no detailed structural data were available.[48] Thus, there still exists the need to obtain the structural details of these **UOH-Ba** phases, along with their derived CDA values, in order to provide an insight into their alteration pathways towards the safe management of SNF *via* long-term disposal in the geological repository.

The search for these intermediate **UOH-Ba** phases was carried out in this project using hydrothermal synthesis, which resulted in the successful formation of two new **UOH-Ba** compounds. Importantly, the crystal structures of both compounds were obtained with synchrotron single-crystal X-ray diffraction and verified by powder X-ray and/or electron diffractions. Whereas the **UOH-Ba1** compound forms a unique corrugated layered structure with interlayer Ba^{2+} ions, the **UOH-Ba2** is made up of a complex 1D and 2D arrays of both pentagonal and tetragonal uranyl polyhedra forming narrow opened channels which house the Ba^{2+} ions. Diffuse reflectance spectroscopy further confirmed the existence of pentavalent uranium in an octahedral coordination environment in **UOH-Ba2**. The results from this work, together with existing literature, provide a foundation to enhance our current understanding in the possible alteration pathway of SNF when in contact with a fluid containing Ba^{2+} ions under an oxidative environment.

2. Experimental

2.1. Materials synthesis

In the literature, a few UOH minerals are known to contain Ba^{2+} ions, major in bauranoite, billietite and protasite, and minor in calciouranoite, meta-calciouranoite, and wölsendorfite.[43–47] However, the UOH minerals can provide only limited structural information on the role of Ba^{2+} ions in the natural weathering of uraninite and the subsequent formations of various uranyl minerals. More detailed structural understanding requires further studies through synthetic phases. Unfortunately, only one synthetic compound with the general formula of $BaU_2O_7(H_2O)_3$ (refer

Table 1 Summary of synthetic UOH compounds with Ba^{2+} ions

		Synthesis conditions		Final product			
			Temp.			U/Ba	
Compound	Precursors	U/Ba	Time	Formula	pH	O/OH	Ref
UOH-Ba	$(UO_2)_8O_2(OH)_{12}\cdot 12H_2O$ $Ba(NO_3)_2$	1/1	200 °C 10 h	$BaU_2O_7(H_2O)_3$	—	2 —	48
UOH-Ba1	U_3O_8 $Ba(NO_3)_2$ and Na_2CO_3	1/2	240 °C 24 h	$Ba(H_2O)_2[(UO_2)_4O_3(OH)_4]$	3.62	4 2.75	This work
UOH-Ba1s	$(UO_2)_8O_2(OH)_{12}\cdot 12H_2O$ $Ba(NO_3)_2$	1/2	240 °C 72 h	$Ba(H_2O)_2[(UO_2)_4O_3(OH)_4]$	—	42.75	This work
UOH-Ba2	$UO_2(NO_3)_2\cdot 6H_2O$ $Ba(NO_3)_2$ and NaOH	1/1	240 °C 24 h	$Ba_2[(UO_2)_{10}UO_{12}(OH)_6\ (H_2O)_{2.5}]$	3.51	5.5 5.25	This work

to **UOH-Ba** in Table 1) was made *via* a hydrothermal reaction of schoepite and barium nitrate solution at 200 °C.[48] Although it was characterised by elemental analysis, PXRD and TGA, crystal structure data were not available.

Schoepite $[(UO_2)_8O_2(OH)_{12}\cdot 12H_2O]$,[49] uranium oxide ($U_3O_8$) and uranyl nitrate hexahydrate with natural uranium isotopic abundance were used as the uranium precursors. Compounds containing uranium are radioactive and should be handled in the regulated laboratories. Other chemicals in A. R. grade were purchased from Sigma-Aldrich (Merck).

2.1.1. Synthesis of $Ba(H_2O)_2[(UO_2)_4O_3(OH)_4]$ (UOH-Ba1). Uranium oxide U_3O_8 (0.0905 g, 0.11 mmol) and $Ba(NO_3)_2$ (0.1582 g, 0.60 mmol) were added to a glass vial with 5 mL of deionized water (DIW), and then mixed with 5 mL of $NaCO_3$ solution (1 mM) under stirring. The mixture was transferred into a 30 mL Teflon vessel, sealed in a steel autoclave, heated in an oven at 240 °C for 24 h, and then cooled to room temperature at 5 °C h^{-1}. An orange needle crystalline product of compound **UOH-Ba1** (0.0939 g, >85 wt% of yield) was obtained from the liquid with the final pH of 3.62 and dried at 50 °C in air. Compound **UOH-Ba1** was also successfully synthesised using schoepite as a uranium precursor [Schoepite (0.1005 g, 0.32 mmol), $Ba(NO_3)_2$ (0.1581 g, 0.60 mmol) in 5 mL of DIW] under the similar hydrothermal conditions (240 °C for 72 h) as a needle crystalline product, refer to **UOH-Ba1s**, with a good yield (0.0942 g, >89%).

2.1.2. Synthesis of $Ba_2(H_2O)[(UO_2)_{10}UO_{12}(OH)_6(H_2O)_2]$ (UOH-Ba2). Uranyl nitrate hexahydrate (0.0504 g, 0.1 mmol) and barium nitrate $Ba(NO_3)_2$ (0.0261 g, 0.1 mmol) were dissolved in 10 mL of DIW. The solution pH was adjusted to 4.50 by adding dilute NaOH solution (1 mM) under stirring, then transferred into a 30 mL Teflon vessel and sealed in a steel autoclave, heated in an oven at 240 °C for 24 h. It was then cooled slowly to room temperature at 5 °C h^{-1}. An orange block crystalline product of compound **UOH-Ba2** (0.0266 g, 82 wt% of yield) was obtained and dried at 50 °C in air.

2.2. Materials characterization

2.2.1. Powder X-ray diffraction. The powder X-ray diffraction (PXRD) data were collected on a Bruker D8 Focus diffractometer (Bruker Corporation, USA) equipped with Cu–Kα (λ = 1.5418 Å) radiation, in the range $5^\circ < 2\theta < 80^\circ$, with a step size of 0.02° (2θ) and an acquisition time of 2 s per step.

2.2.2. Scanning and transmission electron microscopies. A Zeiss Ultra Plus SEM (Carl Zeiss NTS GmbH, Oberkochen, Germany) was operated under an accelerating voltage of 15 kV to check crystalline morphologies and determine the U : Ba ratios. Transmission electron microscopy (TEM) analysis was carried out with a JEOL 2200FS (JEOL Ltd, Japan) operated at 200 kV, fitted with an Oxford X-Max silicon drift detector for Energy Dispersive X-ray analysis (EDX). TEM specimens were prepared by crushing crystalline compounds in ethanol and dispensing them on holey carbon supported films.

2.2.3. Raman spectroscopy. Raman spectra were collected on a Renishaw inVia spectrometer (Renishaw, UK) equipped with a 785 nm excitation Ar laser in the range of 1000–100 cm^{-1} with a spectral resolution of ~1.7 cm^{-1}.

2.2.4. Diffuse reflectance spectroscopy. Diffuse reflectance spectra in both UV-vis and NIR regions were measured on an Agilent Cary 5000 spectrophotometer (Agilent Technologies, USA), equipped with a Labsphere Biconical Accessory and referenced to a Labsphere certified standard (Spectralon).

2.2.5. Thermogravimetric stability. Thermogravimetric analysis (TGA) measurements were carried out on a SEIKO 6300 Thermal Analyzer (SEIKO Instrument Inc., Japan) at a heating rate of 10 °C min^{-1} and an air or argon flow rate of 300 cm^3 min^{-1}.

2.3. Synchrotron single crystal X-ray diffraction

The single crystal data for **UOH-Ba1** (CSD-2247026) and **UOH-Ba2** (CSD-2247027) were collected at 100(2) K on the MX2 beamline[50] at the Australian Synchrotron employing silicon double crystal monochromated synchrotron radiation (λ = 0.71078–0.71093 Å). Data integration and reduction were undertaken with XDS.[51] SADABS was applied to the data for absorption corrections.[52] The structures were solved by direct methods[53] and refined with SHELXL-2014[54] using the Olex^2 graphical user interface.[55] All atoms except hydrogen were located on the electron density maps and refined anisotropically. Hydrogen atoms on possible hydroxyl groups and water molecules were unable to be located and thus were omitted in the final structure refinements. Note the diffraction data for **UOH-Ba1** could be indexed to either the monoclinic or triclinic space groups. However, the subsequent structure refinement for the monoclinic structure did not make chemical sense. So the final crystal structure was refined in the triclinic $P\bar{1}$ space group. The data completeness was a bit low due to only one-circle data collection possible.

3. Results and discussion

3.1. Synthesis and characterization

In this work, two new UOH compounds were successfully synthesised hydrothermally at 240 °C. Compound **UOH-Ba1** was synthesised using a mixture of U_3O_8 and $Ba(NO_3)_2$ in water and pH adjusted with Na_2CO_3. It was also synthesised *via* a hydrothermal reaction of schoepite and $Ba(NO_3)_2$. On the other hand, compound **UOH-Ba2** was made by a hydrothermal reaction of $UO_2(NO_3)\cdot 6H_2O$ and $Ba(NO_3)_2$, with pH adjusted by adding a diluted NaOH solution. Both **UOH-Ba1** and **UOH-Ba2** formed in solutions with a narrow range of final solution pH 3.62 and 3.51, respectively, underpinning the importance of solution pHs in governing the uranyl hydrolysis and subsequent effects on the formation of synthetic UOH phases.[14] However, uranium precursors also affect solution pH and uranium hydrolysis, further influencing the formation and structure of the final UOH phases. The synthetic UOH phases with Ba^{2+} ions discussed above, together with synthesis conditions are summarised in Table 1.

Both compounds were subsequently characterised for structure, microstructure, and elemental ratios. PXRD patterns of both compounds matched the simulated patterns calculated from their single crystal data (Fig. S1, ESI†), confirming that pure phase materials were obtained. The backscattered SEM images (Fig. 2) showed a needle (**UOH-Ba1**) or a block (**UOH-Ba2**) crystal morphology, different from the previously reported thin-plate crystal morphology for layer structured UOH compounds.[31–33] SEM-EDS multipoint analyses confirmed that they contain U, Ba, and O with the U/Ba ratio of 4 and 5.5 for **UOH-Ba1**/**UOH-Ba1s** and **UOH-Ba2**, respectively (Fig. S2–S4, ESI†).

3.2. Crystal structures and discussion

The single crystal data and structural refinement details for both compounds are summarised in Table 2, with selected bond lengths and angles listed in Tables S1–S2, ESI.† Compound **UOH-Ba1** crystallises in the triclinic $P\bar{1}$ space group. The crystal structure is constructed with undulating uranyl oxide hydroxide layers with interlayer hydrated Ba^{2+} ions (Fig. 3). There are two unique uranyl moieties (U1 and U2) in pentagonal bipyramidal polyhedrons, with the U═O bond lengths ranging from 1.77(3) to 1.79(4) Å and O═U═O angles from 176.3(18)° to 177.3(17)°.

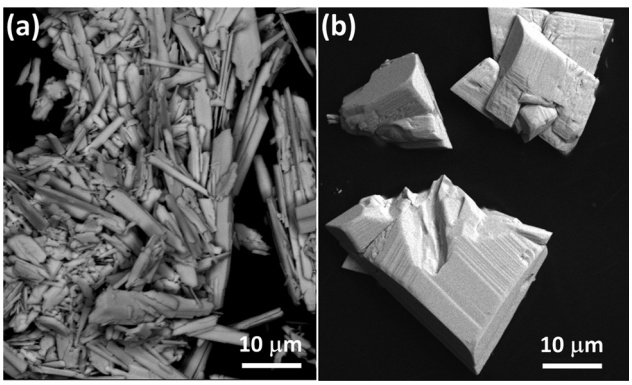

Fig. 2 Backscattered SEM images of **UOH-Ba1** (a) and **UOH-Ba2** (b).

The U–O bond lengths in the equatorial planes range from 2.20(4) to 2.37(4) Å (Table S1, ESI†). These typical U═O and U–O bonds for the uranyl moieties are similar to other compounds containing uranyl ions such as UOH minerals and synthetic compounds.[56] Either U1 or U2 polyhedrons share edges to form 1D zigzag arrays that are connected to each other repeatedly *via* corner-sharing between the two types of arrays to form the corrugated uranyl oxide hydroxide layers with interlayer Ba^{2+} ions (Fig. 3). The Ba^{2+} ions are 11-fold coordinated with seven uranyl O atoms (O1/O1′/O2/O2′/O4/O4′/O5), two equatorial O atoms (O3 and O6), and two H_2O molecules (O9/O9′), with Ba–O bonds ranging from 2.72(3) to 3.08(3) Å for uranyl O atoms, 3.26(4) to 3.29(3) Å for equatorial O atoms and 2.865(5) to 2.869(5) Å for H_2O molecules (Table S1, ESI†). Note the relatively longer Ba–O distances for the equatorial O atoms (O3 and O6) are just beyond the normal Ba–O bond range, suggesting weak bonding nature. Such weak bonding between equatorial O atoms and interlayer cations are unique and can exist only in layered UOH compounds with corrugated uranyl oxide hydroxide layers.

Compound **UOH-Ba2** crystallises in the monoclinic $C2/c$ space group. The complex 3D structure comprises of six unique uranium centres, four (U2-U5) in pentagonal bipyramids, one (U1) in a square bipyramid, and one (U6) in an octahedral geometry (Fig. 4). The crystal structure is constructed as stacking of multiple layers of three different building arrays repeatedly, parallel to the (001) plane (Fig. 4a and b). The first 1D chains are formed by edge-sharing of double U1 and U2 polyhedra (Fig. 4c). The second 1D chains are formed by corner-sharing of a repeated edge-sharing U3–U4 pairs (Fig. 4d). The third 2D nets are formed by corner-sharing of U5 and U6 polyhedra at an angle of approximate 76.786° with each U5 linking to two U6 and each U6 linking to four U5 (Fig. 4e and f). The 2D nets are linked to the 1D arrays of U3–U4 pairs on both sides, with one side rotating 90° forming the sandwich-type structural building blocks that are linked between 1D arrays of U3–U4 and U1–U2 (Fig. 4c), *via* the parallel 1D arrays of U1–U2 by rotating 90° constantly (Fig. 4a and b). The 1D arrays of U3–U4 are connected by the 1D arrays of U1–U2 *via* uranyl cation–cation interactions resulting in a tilting of approximately 115°. The overall structure could be simplified as layers of U3-U4 and U5-U6 sandwiching layers of U1-U2 to form a 3D open framework, with Ba^{2+} ions in the narrow channels (Fig. 4a and b).

For uranyl U2–U5, the U═O bond lengths range from 1.773(7) to 1.828(7) Å with O═U═O angles from 176.7(3) to 178.7(3)°, and U–O bond lengths in the equatorial planes ranging from 2.196(7) to 2.583(7) Å (Table S2, ESI†). For U1 a in square bipyramid, U═O bond lengths are 1.838(7) and 1.841(7) Å with the O═U═O angle of 175.9(3)°, and U–O bond lengths in the equatorial plane from 2.139(7) to 2.422(7) Å. The U6 does not show a uranyl centre and it has an octahedral coordination environment with six U–O bonds from 2.052(7) to 2.102(7) Å. The Ba^{2+} ion is in a 10-fold coordination environment, eight uranyl O atoms with Ba–O bond lengths from 2.717(7) to 2.947(8) Å, and two H_2O molecules with Ba–O bond lengths of 3.073(7) and 3.306(6) Å (Table S2, ESI†). The longer than normal

Table 2 Crystal data and structure refinement for **UOH-Ba1** and **UOH-Ba2**

Compounds	**UOH-Ba1**	**UOH-Ba2**
Empirical formula	$BaO_{17}U_4$	$Ba_2O_{40.50}U_{11}$
Formula weight	1361.46	3541.01
Temperature/K	100(2)	100(2)
Crystal system	Triclinic	Monoclinic
Space group	$P\bar{1}$	$C2/c$
a/Å	4.2320(9)	13.251(3)
b/Å	8.1990(16)	10.389(2)
c/Å	10.649(2)	25.130(5)
α/°	87.40(3)	—
β/°	78.01(3)	90.33(3)
γ/°	75.01(3)	—
Volume/Å^3	349.79(14)	3459.5(12)
Z	1	8
ρ_{calc}/g cm^{-3}	6.463	6.799
μ/mm^{-1}	49.001	53.640
F(000)	560.0	5792.0
Radiation	Synchrotron (λ = 0.71093)	Synchrotron (λ = 0.71078)
2θ range for data collection/°	3.904 to 49.928	3.242 to 51.996
Index ranges	$-4 \le h \le 4$, $-9 \le k \le 9$, $-12 \le l \le 12$	$-15 \le h \le 15$, $-12 \le k \le 12$, $-29 \le l \le 29$
Reflections collected	3822	21 522
Independent reflections	1079 [R_{int} = 0.0601, R_{sigma} = 0.0630]	3316 [R_{int} = 0.0516, R_{sigma} = 0.0325]
Data/restraints/parameters	1079/105/94	3316/309/236
Goodness-of-fit on F^2	1.143	1.092
Final R indexes [$I >= 2\sigma(I)$]^a	R_1 = 0.0812, wR_2 = 0.2197	R_1 = 0.0295, wR_2 = 0.0751
Final R indexes [all data]^a	R_1 = 0.1128, wR_2 = 0.2902	R_1 = 0.0303, wR_2 = 0.0757
Largest diff. peak/hole/e Å^{-3}	4.84/−4.59	3.49/−3.10

^{a} $R_1 = \Sigma||F_o| - |F_c||/|F_o|$; $wR_2 = \{\Sigma[w(F_o^2 - F_c^2)^2]/\Sigma[w(F_o^2)^2]\}^{1/2}$.

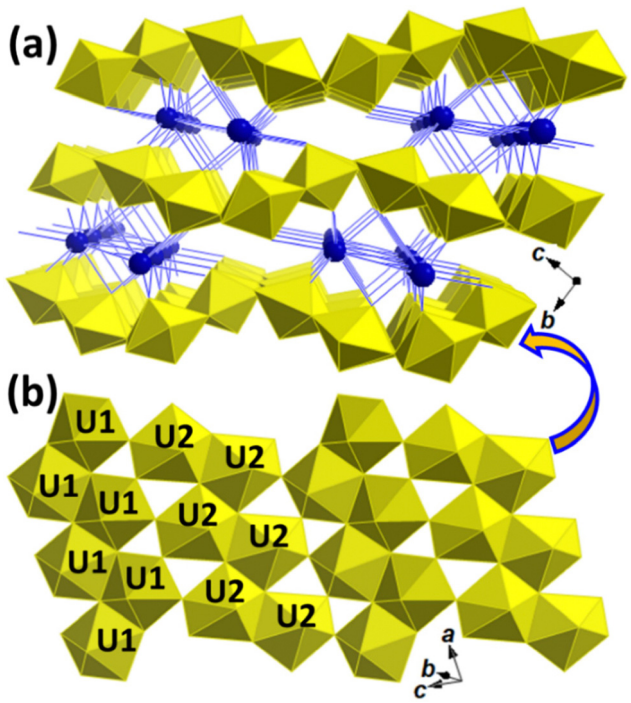

Fig. 3 Crystal structure of compound **UOH-Ba1**: a 2D layered structure with interlayer Ba^{2+} ions (a), and two types of pentagonal bipyramidal uranium polyhedrons (U1 and U2) linking into the corrugated uranyl oxide hydroxide layers (b).

Ba–O bond range exists for O21, a disordered H_2O molecule in two partially occupied positions.

The bond valence sums (BVS)[56,57] were calculated using U^{6+} parameters (R_{U-O} = 2.051; B = 0.519),[57] with BVS results for both compounds listed in Tables S3–S4 (ESI†). The BVS values for **UOH-Ba1** (6.60 for U1, 6.59 for U2 and 2.14 for Ba1 in Table S3, ESI†) suggest hexavalent uranium for uranyl groups and Ba^{2+} ion. In addition, majority of O atoms are O, with OH for O7 and O8, and H_2O for O9. The unit cell contains four uranyl units (2U1 and 2U2), one Ba^{2+} ion, three O (O3 and O6), four OH^- (2O7 and 2O8) and two coordinated H_2O molecules (2O9), leading to the formula $Ba(H_2O)_2[(UO_2)_4O_3(OH)_4]$. While four uranium centres (U2-U5) in **UOH-Ba2** are indicative of hexavalent, both U1 and U6 in 8-fold coordination may be in pentavalent state with BVS values of 5.66 and 5.78 (Table S4, ESI†). The BVS values also suggest Ba^{2+} (2.21) and majority of O atoms as O, with OH for O3, O13 and O17, and H_2O for O9 and O21. The presence of U(v) in the octahedral environment was confirmed using DRS (Section 3.5 below). The unit cell contains 8 Ba^{2+} ions, 44 U (40 uranyl units and 4 octahedrons), 164 O (128 O, 24 OH and 12 H_2O), leading to the formula $Ba_2(H_2O)[(UO_2)_{10}UO_{12}(OH)_6(H_2O)_2]$.

So far, three UOH minerals incorporating only Ba^{2+} ions in their crystal structures have been identified, demonstrating the importance of Ba^{2+} ions in the natural weathering of uraninite. Protasite and billietite were first reported in 1987,[43] with billietite structure being revisited in 2006.[44] However, crystal structure of mineral bauranoite ($Ba[(UO_2)(O,OH)](H_2O)_{4.5}$) remains unknown.[45] While protasite contains the α-U_3O_8 type uranyl oxide hydroxide layers (Fig. 5a) with interlayer hydrated Ba^{2+} ions, billietite adopts both the α-U_3O_8 and β-U_3O_8 uranyl oxide hydroxide layers (Fig. 5c). In contrast to the two known UOH minerals with Ba^{2+} ions, the uranyl oxide hydroxide layers

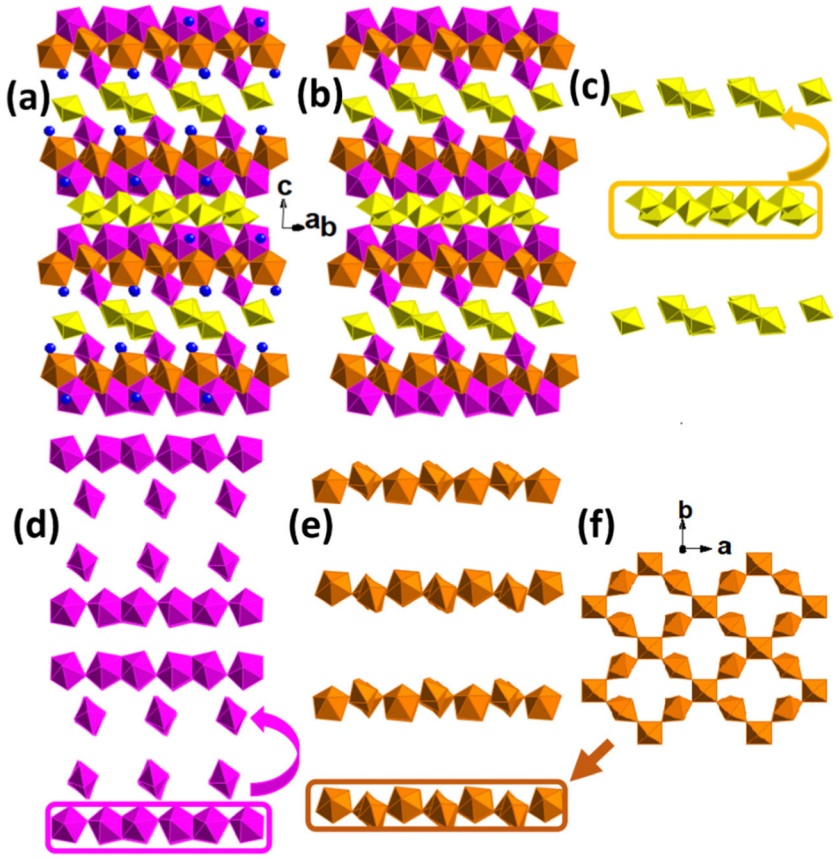

Fig. 4 Crystal structure of **UOH-Ba2**: overall 3D polyhedral crystal structure (a), the same as in (a) but without Ba^{2+} ions (b), double U1 and U2 edge-sharing to form Zigzag 1D chains (c), pairs of edge-sharing U3 and U4 connected by corner-sharing to form 1D chains (d), U5 and U6 connected by corner-sharing to form 2D nets [(e) and (f)]. Uranium polyhedrons: U1 and U2 are in yellow, U3 and U4 in scarlet, U5 and U6 in orange; Ba in blue spheres.

for compound **UOH-Ba1** contains two types of pentagonal pyramidal uranyl polyhedrons linking parallelly to form opposite distorted triangles between them in zigzag pattern (Fig. 5b). As such, **UOH-Ba1** has corrugated uranium oxide hydroxide layers that is not common but observed previously in UOH mineral curite[58] and a few synthetic UOH compounds such as $Na[(UO_2)_4O_2(OH)_5](H_2O)_2$[59] and $Ca(UO_2)_4O_3(OH)_4(H_2O)_2$.[25]

In the literature, two synthetic UOH compounds (**UOH-Sr**[60] and **UOH-Pb**[27]) were found to have the similar 3D structures with **UOH-Ba2** and their structural similarities and differences are summarised in Table 3. Apart from having the same monoclinic *C*2/*c* space group and similar cell parameters, the obvious difference is the smaller β angle for **UOH-Ba2** (90.33°) in comparison to around 103.20° for **UOH-Pb** and **UOH-Sr.** It is also interesting to note that only 2+ metal ions with relatively large ionic radii (1.35–1.52 Å) such as Pb^{2+}, Sr^{2+} and Ba^{2+} can stabilise this structure type. It seems to suggest that the larger 2+ metal ions allow high coordination numbers (9 to 10), which may be the key factor for stabilising such a complex 3D structure, highlighting the complexity and flexibility of UOH systems in the presence of larger 2+ metal ions. As U(v) in the octahedral coordination environment was confirmed for both

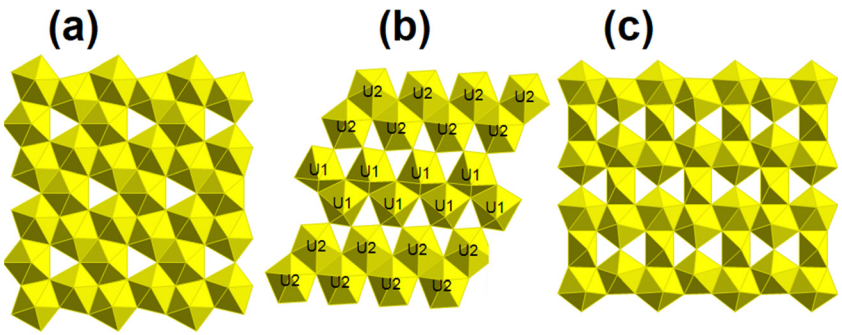

Fig. 5 Polyhedral uranyl oxide hydroxide layers: α-U_3O_8 type layer in protasite (a), **UOH-Ba1** (b), and β-U_3O_8 layer in billietite (c).

UOH-Sr and **UOH-Ba2**, it is very likely that **UOH-Pb** would have the U(v) centre as well.

3.3. Transmission electron microscopy

Compound **UOH-Ba1** was further studied by TEM. The key elements of U, Ba and O were confirmed by TEM-EDS. Bright field TEM images of **UOH-Ba1** (Fig. 6a and b) showed long needle crystals. Selected area electron diffraction (SAED) patterns in [−1 −1 −1] zone axis (Fig. 6c) and [2 −1 −1] zone axis (Fig. 6d) were both indexed to triclinic $P\bar{1}$ space group, consistent with the results from single crystal and powder XRD.

3.4. Electronic structures and uranium valences

As the calculated BVS values indicating the possible presence of pentavalent uranium in the octahedral coordination site in **UOH-Ba2**, the electronic structures were investigated by DRS. The DRS spectra of **UOH-Ba1** and **UOH-Ba2** in the UV-vis region (Fig. 7) showed the similar strong and broad absorption bands reflecting the charge transfer feature for U(vi) ions.[61,62] However, the spectra in the near infrared (NIR) region clearly showed the presence of pentavalent U in **UOH-Ba2** as the sharp absorption band at 1448 nm due to U(v) ion in $5f^1$ configuration.[63–66] The absorption band (1448 nm) is very close to the value (1445 nm) observed for the non-uranyl U(v) centre in an octahedral coordination environment,[64] consistent with the crystallographic result in this work. In contrast, U(v) in an 8-fold coordination environment would give the absorption band at much longer wavelengths (~1615).[67] Note the presence of U(v) in several oxides including minerals and synthetic compounds were reported earlier, but none of them contain pentavalent uranyl ion.[68] The weak and broad absorption for **UOH-Ba1** in the same area was due to the presence of H_2O molecules. As such, **UOH-Ba2** is a UOH compound with mixed U valences, major in U(vi) and minor in U(v). Mixed uranium valences are rarely observed in UOH systems,[40,69] and a complex 3D UOH structure with mixed-valence uranium in **UOH-Ba2** would be rather rare.

3.5. Vibrational modes

Raman spectroscopy was used to probe the vibrational modes. Similar to earlier studies, the signature vibrations for both **UOH-Ba1** and **UOH-Ba2** (Fig. 8) arise from the uranyl vibrations, with $\nu_1(UO_2)^{2+}$ in strong and sharp peaks between 700 and 900 cm^{-1}, $\nu(U_3O)$ and $\gamma[U_3(OH)_3]$ in medium and broad peaks at 300 to 600 cm^{-1}, $\nu_2(UO_2)^{2+}$ in weak and broad peaks at 200 to 300 cm^{-1} and lattice vibrations at ≤150 cm^{-1}.[70–72] It is apparent that $\nu_1(UO_2)^{2+}$ vibrations split in both compounds reflecting the subtle differences in uranyl moieties. For **UOH-Ba1**, the three $\nu_1(UO_2)^{2+}$ vibrations at 779.6 cm^{-1} (strong), 799.5 cm^{-1} (weak) and 834.6 cm^{-1} (strong) correspond to the estimated U═O bond lengths of 1.78 to 1.83 Å.[71] In contrast, **UOH-Ba2** shows multiple splitting bands for $\nu_1(UO_2)^{2+}$ vibrations, at 740.2 cm^{-1} (weak), 774.8 cm^{-1} (strong), 809.4 cm^{-1} (strong), and 875.0 cm^{-1} (weak), corresponding to the calculated U═O bond lengths of 1.88, 1.84, 1.80 and 1.74 Å, respectively.[73] These inferred U═O bond values from the Raman vibrations are broadly consistent with the crystal structures with U═O bond lengths ranging from 1.773(7) to 1.841(7) Å.

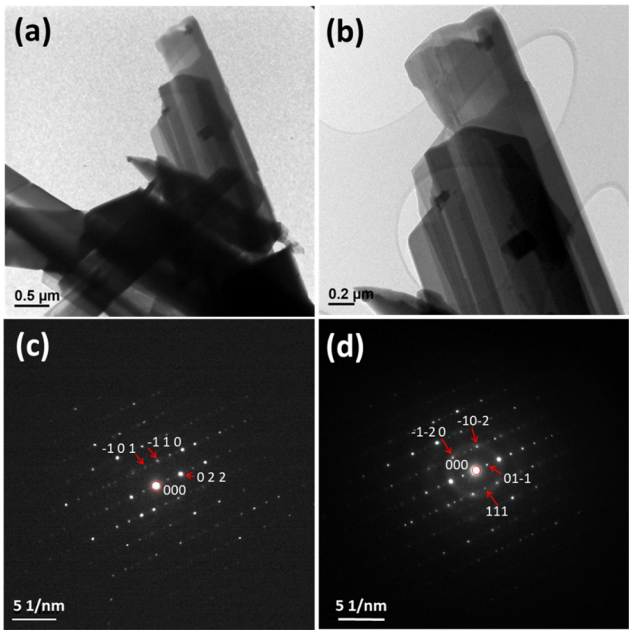

Fig. 6 TEM of **UOH-Ba1**: A bright field TEM image (a), a TEM image showing grains in higher magnification (b), SAED patterns from a grain in [−1 −1 −1] zone axis (c) and a grain in [2 −1 −1] zone axis (d) indexed to the $P\bar{1}$ space group.

3.6. Thermal stability

The thermal stability of **UOH-Ba1** was further investigated. Based on the thermogravimetric and differential thermal analysis results (Fig. S5, ESI†), the thermal decomposition of compound **UOH-Ba1** went through a few steps: (1) gradually lost half lattice H_2O molecules from 50 to 240 °C with an endotherm at 135 °C (calc. 0.66%, measured 0.6%); (2) lost all H_2O molecules and three OH groups from 240 °C to 600 °C in two steps (calc. 5.74%, measured 5.7%); (3) lost final O through UO_3 to UO_{2+x} reduction

Table 3 Crystal and chemical comparisons of **UOH-Ba2** with similar structured **UOH-Sr** and **UOH-Pb** compounds

Synthetic phase and formula	Structure	Cell parameters	[n]M	M-ionic radii (Å)	M–O (Å)	U(v)
UOH-Pb[27] $Pb_2(H_2O)[(UO_2)_{10}UO_{12}(OH)_6(H_2O)_2]$	$C2/c$	a = 13.281(5), b = 10.223(4), c = 26.10(1) Å; β = 103.202(6)°	[9]	1.35	2.53(3) –3.07(3)	—
UOH-Sr[60] $Sr_2(H_2O)[(UO_2)_{10}UO_{12}(OH)_6(H_2O)_2]$	$C2/c$	a = 13.289(3), b = 10.170(2), c = 26.139(5) Å; β = 103.04(3)°	[10]	1.36	2.574(18)–3.004(10)	yes
UOH-Ba2 (this work) $Ba_2(H_2O)[(UO_2)_{10}UO_{12}(OH)_6(H_2O)_2]$	$C2/c$	a = 13.251(3), b = 10.389(2), c = 25.130(5) Å; β = 90.33(3)°	[10]	1.52	2.717(7)–3.306(6)	yes

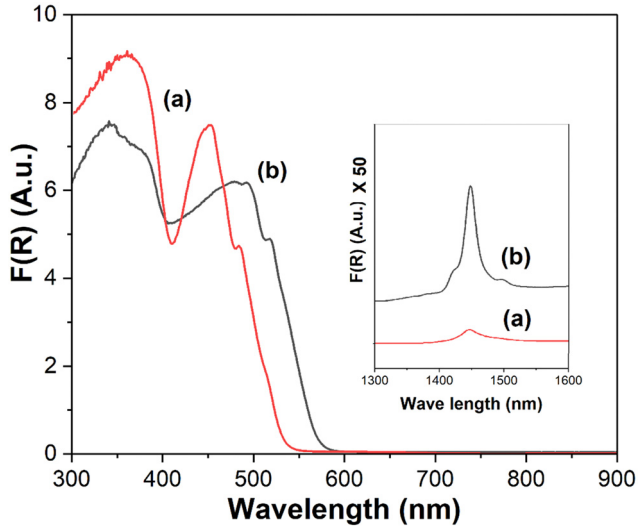

Fig. 7 DR spectra of **UOH-Ba1** (a) and **UOH-Ba2** (b) with an inset of the spectra in the near infrared regain (1300 to 1600 nm).

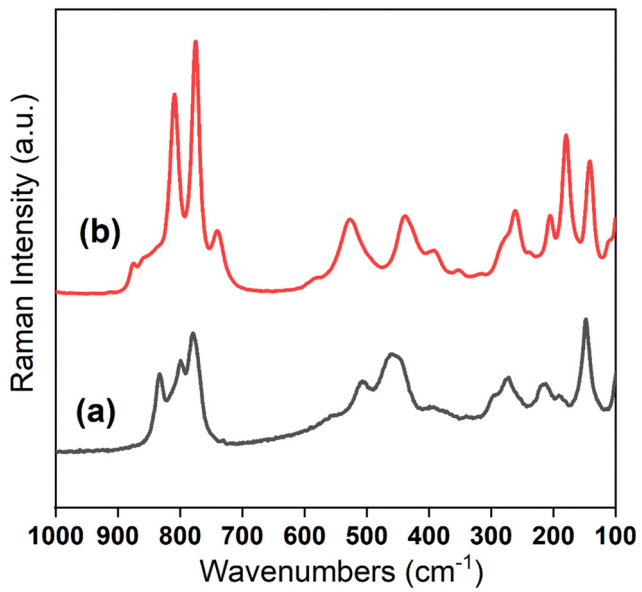

Fig. 8 Raman spectra of **UOH-Ba1** (a) and **UOH-Ba2** (b).

from 800 to 900 °C, with the final residue ($BaUO_4$ + U_3O_7) (calc. 93.0%, measured 93.5%).

3.7. Implications

The charge deficiency per anion (CDA) is a measure of the charge imbalance in the structural units of UOH minerals. As these minerals undergo alteration starting from uraninite, the CDA value increases. The CDA value is closely tied to the average coordination number of oxygens in the structural unit and plays a vital role in determining the crystal-chemical properties of UOH minerals, such as the pH of the liquids they can crystallise in.[14] The CDA values, in combination with the U/OH and Me/U ratios, are used to assess the degree of alteration in UOH minerals.

Although having more secondary cations in the structure, compound **UOH-Ba1** has a CDA value of 0.19, in between the values for billietite (0.15) and protasite (0.22), indicating that it is in between the two minerals in terms of alterations from uraninite. Compound **UOH-Ba2** on the other hand has the same CDA value (0.14), the U/OH ratio (1.83), and the Me/U ratio (0.18) to those of compounds **UOH-Sr**[60] and **UOH-Pb**,[27] indicating they could be of the same alteration stage during the oxidative weathering of uraninite.

A weathering path could be seen based on the CDA values of all UOH minerals and synthetic compounds with Ba^{2+} ions, together with selected UOH minerals (Table 4). An oxidative alteration of SNF starts from UO_2 (similar to uraninite) to a mixed valence uranium in **UOH-Ba2** with CDA = 0.14 similar to billietite with CDA = 0.15 by gradually taking in Ba^{2+} ions and balanced by the rearrangement of the pentagonal and square uranyl bipyramidal polyhedra. Up on further alteration, all square bipyramidal uranyl ions transform into pure pentagonal bipyramidal polyhedra while taking in even more interlayer cations resulting in compound **UOH-Ba1** with CDA = 0.19. The final stage involves the rearrangement of the pentagonal uranyl polyhedra resulting in a stable α-U_3O_8 type structure in protasite with CDA = 0.22. However, this is only the observation from the limited information on synthetic UOH materials. The presence of U centres in the square bipyramidal coordination environment among uranyl phosphate hydrate minerals such as autunite ($Ca[(UO_2)(PO_4)]_2{\cdot}10–12H_2O$)[74] clearly highlights the importance of thermodynamic and kinetic factors in controlling the formation of other types of uranyl minerals and synthetic phases.

Hydrothermal synthesis in the laboratory has shown to be an important method in closing the knowledge gap that is critical to the understanding of the oxidative weathering of UO_2 both as mineral uraninite and SNF. The successful synthesis and characterisation of **UOH-Ba1** and **UOH-Ba2** have filled in the knowledge gaps in the structural understanding on the formation of UOH phases in the presence of Ba^{2+} ions. This work further reinforces that solution pH plays a vital role in controlling uranium hydrolysis and subsequent formation of UOH phases. Besides, the choice of uranium and secondary metal precursors also affects solution pH value, metal ion hydrolysis speciation and the final product. It is anticipated that a reasonably well designed UOH system can lead to the formation of a variety of UOH products with chosen secondary metal ions, leading to an improved fundamental understanding of potential alteration of SNF under long-term storage/disposal in a geological repository.

4. Conclusions

The primary aim of this work was to reveal the missing structural links in the **UOH-Ba** system, subsequently to improve our intrinsic understanding the role of Ba^{2+} ions in the natural weathering and oxidative-hydrolysis alteration of SNF in long-term storage and geological disposal. Consequently, two new synthetic UOH compounds with Ba^{2+} ions were successfully

Table 4 Structural units and structural-chemical characteristics (CDA – charge deficiency per anion; Me/U – metal to U ratio; [*n*]U – average U coordination number) for selected UOH minerals and synthetic compounds

UOH minerals and formula[14]	Structural unit	CDA[a]	U/OH	Me/U	[*n*]U
Schoepite $[(UO_2)_4O(OH)_6](H_2O)_6$	$[(UO_2)_4O(OH)_6]^0$	0.08	0.67	0	[7]
Vandendriesscheite $Pb_{1.5}[(UO_2)_{10}O_6(OH)_{11}](H_2O)_{11}$	$[(UO_2)_{10}O_6(OH)_{11}]^{3-}$	0.14	0.91	0.150	[7]
Becquerelite $Ca[(UO_2)_3O_2(OH)_3]_2(H_2O)_8$	$[(UO_2)_3O_2(OH)_3]^{1-}$	0.15	1.00	0.333	[7]
Gauthierite $KPb[(UO_2)_7O_5(OH)_7](H_2O)_8$	$[(UO_2)_7O_5(OH)_7]^{3-}$	0.17	1.00	0.256	[7]
Fourmarierite $Pb[(UO_2)_4O_3(OH)_4](H_2O)_4$	$[(UO_2)_4O_3(OH)_4]^{1-}$	0.19	1.00	0.250	[7]
Masuyite $Pb[(UO_2)_3O_3(OH)_2](H_2O)_3$	$[(UO_2)_3O_3(OH)_2]^{2-}$	0.22	1.50	0.333	[7]
Curite $Pb_3(H_2O)_2[(UO_2)_8O_8(OH)_6](H_2O)_5$	$[(UO_2)_8O_8(OH)_6]^{6-}$	0.24	1.33	0.375	[6]/[7]
Spriggite $Pb_3[(UO_2)_6O_8(OH)_2](H_2O)_3$	$[(UO_2)_6O_8(OH)_2]^{6-}$	0.29	3.00	0.500	[6]/[7]
Billietite $Ba[(UO_2)_3O_2(OH)_3]_2(H_2O)_4$	$[(UO_2)_3O_2(OH)_3]^{1-}$	0.15	1.00	0.333	[7]
Protasite $Ba[(UO_2)_3O_3(OH)_2](H_2O)_3$	$[(UO_2)_3O_3(OH)_2]^{2-}$	0.22	1.50	0.333	[7]
Synthetic UOH compounds	**Structural unit**	**CDA[a]**	**U/OH**	**Me/U**	**[*n*]U**
UOH-Pb[27] $Pb_2(H_2O)[(UO_2)_{10}UO_{12}(OH)_6(H_2O)_2]$	$[(UO_2)_{10}UO_{12}(OH)_6]^{4-}$	0.14	1.83	0.18	[6]/[7]
UOH-Sr[60] $Sr_2(H_2O)[(UO_2)_{10}UO_{12}(OH)_6(H_2O)_2]$	$[(UO_2)_{10}UO_{12}(OH)_6]^{4-}$	0.14	1.83	0.18	[6]/[7]
UOH-Ba1 (this work) $Ba[(UO_2)_4O_3(OH)_4](H_2O)_2$	$[(UO_2)_4O_3(OH)_4]^{2-}$	0.19	1.00	0.25	[7]
UOH-Ba2 (this work) $Ba_2[(UO_2)_{10}UO_{12}(OH)_6(H_2O)](H_2O)_{1.5}$	$[(UO_2)_{10}UO_{12}(OH)_6]^{4-}$	0.14	1.83	0.18	[6]/[7]

[a] CDA – charge deficiency per anion: calculated as the effective charge of the structural unit divided by the anions in the structural unit. The effective charge is the formal charge plus the charge contributed by the (H)-bonds in the structural unit = $n \times 0.2$.

synthesised hydrothermally and characterised using a variety of structural and spectroscopic techniques. The crystal structures were determined using synchrotron single-crystal XRD and confirmed with PXRD and/or TEM. Compound **UOH-Ba1** has an undulating layered structure with interlay Ba^{2+} ions while **UOH-Ba2** has a complex 3D structure built up with several types of uranium polyhedra. The presence of pentavalent U in the octahedral coordination environment in **UOH-Ba2** was confirmed with DRS.

The successful synthesis and characterisation of these UOH compounds have unravelled the complexity and flexibility of the uranium oxide hydrate system in the presence of Ba^{2+} ions. The results from the current work, together with the related literature, help not only to improve our fundamental understanding on the possible alteration of SNF but also pave the way for future studies especially on the effect of various synthesis factors such as choices of uranium and secondary metal precursors and controlling of the solution final pH on the formation and structures of UOH phases with other secondary metal ions.

Author contributions

K. T. Lu: data curation, formal analysis, writing – review & editing; Y. Zhang: conceptualization, data curation, formal analysis, project administration, resources, writing – review & editing, supervision; T. Wei: data curation, formal analysis, writing – review & editing; T. A. Ablott: data curation, formal analysis, writing – review & editing; J. Plášil: conceptualization, formal analysis, writing – review & editing; I. Karatchevtseva: data curation, formal analysis, writing – review & editing; R. Zheng: conceptualization, resources, writing – review & editing, supervision.

Conflicts of interest

There are no conflicts to declare.

Acknowledgements

Synthesis and characterisation of materials were performed in the facilities under Nuclear Science and Technology (NST) at ANSTO. The crystallographic data for compounds **UOH-Ba1** and **UOH-Ba2** were collected on the MX2 beamline at the Australian Synchrotron, ANSTO, and made use of the Australian Cancer Research Foundation (ACRF) detector.

References

1 V. Popa and O. Cocoş, *Cent. Eur. J. Geogr. Sustainable Dev.*, 2021, **3**, 17–25.
2 J. Plášil, *J. Geosci.*, 2014, **59**, 99–114.

3 J. Janeczek and R. C. Ewing, *J. Nucl. Mater.*, 1992, **190**, 128–132.
4 S. Spiridonov, A. Perevolotskii, T. Perevolotskaya, R. Aleksakhin and E. Spirin, *At. Energy*, 2017, **123**, 122–126.
5 R. J. Baker, *Coord. Chem. Rev.*, 2014, **266**, 123–136.
6 A. Paulillo, J. M. Dodds, S. J. Palethorpe and P. Lettieri, *Sustainable Mater. Technol.*, 2021, **28**, e00278.
7 D. Mallants, K. Travis, N. Chapman, P. V. Brady and H. Griffiths, *Energies*, 2020, **13**(4), 833.
8 S. El-Showk, *Science*, 2022, **375**, 806–810.
9 R. J. Finch, R. Haddal and G. T. Baldwin, *Safeguards Implications for Deep Borehole Disposal of Spent Fuel, SAND2016-4591 report*, Sandia National Laboratories, USA, 2016.
10 R. C. Ewing, *Nat. Mater.*, 2015, **14**, 252–257.
11 D. J. Wronkiewicz, J. K. Bates, S. F. Wolf and E. C. Buck, *J. Nucl. Mater.*, 1996, **238**, 78–95.
12 R. J. Finch and R. C. Ewing, *J. Nucl. Mater.*, 1992, **190**, 133–156.
13 J. Janeczek and R. Ewing, *J. Nucl. Mater.*, 1992, **190**, 157–173.
14 J. Plášil, *Eur. J. Mineral.*, 2017, **29**, 1–15.
15 P. C. Burns, Hydrated uranium oxides, in *Comprehensive Nuclear Materials*, ed. R. Konings and R. Stoller, Elsevier, 2nd edn, 2020.
16 T. A. Olds, J. Plasil, A. R. Kampf, T. Spano, P. Haynes, S. M. Carlson, P. C. Burns, A. Simonetti and O. P. Mills, *Am. Mineral.*, 2018, **103**, 143–150.
17 P. C. Burns, *Can. Mineral.*, 1998, **36**, 1061–1067.
18 C. L. Cahill and P. C. Burns, *Am. Mineral.*, 2000, **85**, 1294–1297.
19 J. Plášil, R. Škoda, J. Čejka, V. Bourgoin and J.-C. Boulliard, *Eur. J. Mineral.*, 2016, **28**, 959–967.
20 K. A. Hughes, P. C. Burns and U. Kolitsch, *Can. Mineral.*, 2003, **41**, 677–685.
21 J. Plášil, *Eur. J. Mineral.*, 2018, **30**, 237–251.
22 M. L. Miller, R. J. Finch, P. C. Burns and R. C. Ewing, *J. Mater. Res.*, 1996, **11**(12), 3048–3056.
23 P. C. Burns and F. C. Hill, *Can. Mineral.*, 2000, **38**, 163–173.
24 F. C. Hill and P. C. Burns, *Can. Mineral.*, 1999, **37**, 1283–1288.
25 R. E. Glatz, Y. Li, K.-A. Hughes, C. L. Cahill and P. C. Burns, *Can. Mineral.*, 2002, **40**, 217–224.
26 P. C. Burns and F. C. Hill, *Can. Mineral.*, 2000, **38**, 175–181.
27 Y. Li and P. C. Burns, *Can. Mineral.*, 2000, **38**, 1433–1441.
28 M. Rivenet, N. Vigier, P. Roussel and F. Abraham, *J. Solid State Chem.*, 2009, **182**, 905–912.
29 N. G. Chernorukov, O. V. Nipruk, K. A. Klinshova, O. N. Tumaeva and D. V. Sokolov, *New J. Chem.*, 2021, **45**, 9922–9935.
30 T. A. Ablott, K. T. Lu, T. Wei and Y. Zhang, *Dalton Trans.*, 2023, **52**, 6629–6640.
31 Y. Zhang, J. Čejka, G. R. Lumpkin, T. Trong Tran, I. Aharonovich, I. Karatchevtseva, J. R. Price, N. Scales and K. Lu, *New J. Chem.*, 2016, **40**, 5357.
32 Y. Zhang, R. Aughterson, I. Karatchevtseva, L. Kong, T. T. Tran, J. Čejka, I. Aharonovich and G. R. Lumpkin, *New J. Chem.*, 2018, **42**, 12386–12393.
33 Y. Zhang, R. D. Aughterson, Z. Zhang, T. Wei, K. Lu, J. Čejka and I. Karatchevtseva, *Inorg. Chem.*, 2019, **58**, 10812–10821.
34 Y. Zhang, K. T. Lu and R. Zheng, *Dalton Trans.*, 2022, **51**, 2158–2169.
35 Y. Li, C. L. Cahill and P. C. Burns, *Chem. Mater.*, 2001, **13**, 4026–4031.
36 K.-A. Kubatko and P. C. Burns, *Inorg. Chem.*, 2006, **45**, 10277–10281.
37 T. A. Ablott, K. T. Lu, R. D. Aughterson and Y. Zhang, *Dalton Trans.*, 2022, **51**, 15965–15973.
38 K. T. Lu, Y. Zhang, R. D. Aughterson and R. Zheng, *Dalton Trans.*, 2020, **49**, 15854–15863.
39 K. T. Lu, Y. Zhang, T. Wei, Z. Wang, D. T. Oldfield and R. Zheng, *Inorg. Chem.*, 2021, **60**, 13233–13241.
40 Y. Zhang, T. Wei, T. Trong Tran, K. T. Lu, Z. Zhang, J. R. Price, I. Aharonovich and R. Zheng, *Inorg. Chem.*, 2020, **59**, 12166–12175.
41 R. Price, C. Gray, R. Wilson, F. Frey and S. Taylor, *Chem. Geol.*, 1991, **93**, 245–265.
42 I. Sato, H. Furuya, T. Arima, K. Idemitsu and K. Yamamoto, *J. Nucl. Sci. Technol.*, 1999, **36**, 775–780.
43 M. K. Pagoaga, D. E. Appleman and J. M. Stewart, *Am. Mineral.*, 1987, **72**, 1230–1238.
44 R. J. Finch, P. C. Burns, F. C. Hawthorne and R. C. Ewing, *Can. Mineral.*, 2006, **44**, 1197–1205.
45 V. Rogova, L. Belova, G. Kiziyarov and N. Kuznetsova, *Int. Geol. Rev.*, 1974, **16**, 214–219.
46 V. Rogova, L. Belova, G. Kiziyarov and N. Kuznetsova, *Int. Geol. Rev.*, 1974, **16**, 1255–1256.
47 P. C. Burns, *Am. Mineral.*, 1999, **84**, 1661–1673.
48 N. G. Chernorukov, O. V. Nipruk, G. N. Chernorukov, R. V. Abrazheev and K. A. Chaplieva, *Russ. J. Gen. Chem.*, 2019, **89**, 71–75.
49 J. Plášil, *J. Geosci.*, 2018, **63**, 65–73.
50 D. Aragão, J. Aishima, H. Cherukuvada, R. Clarken, M. Clift, N. P. Cowieson, D. J. Ericsson, C. L. Gee, S. Macedo, N. Mudie, S. Panjikar, J. R. Price, A. Riboldi-Tunnicliffe, R. Rostan, R. Williamson and T. T. Caradoc-Davies, *J. Synchrotron Radiat.*, 2018, **25**, 885–891.
51 W. Kabsch, *Acta Crystallogr., Sect. D: Biol. Crystallogr.*, 2010, **66**, 133–144.
52 G. M. Sheldrick, *SADABS, Empirical Absorption and Correction Software*, University of Göttingen, Göttingen, 1996.
53 G. M. Sheldrick, *Acta Crystallogr., Sect. A: Found. Adv.*, 2015, **71**, 3–8.
54 G. M. Sheldrick, *Acta Crystallogr., Sect. C: Struct. Chem.*, 2015, **71**, 3–8.
55 O. V. Dolomanov, L. J. Bourhis, R. J. Gildea, J. A. K. Howard and H. Puschmann, *J. Appl. Crystallogr.*, 2009, **42**, 339–341.
56 I. D. Brown, *Chem. Rev.*, 2009, **109**(12), 6858–6919.
57 P. C. Burns, P. C. Burns, R. C. Ewing and F. C. Hawthorne, *Can. Mineral.*, 1997, **35**, 1551–1570.
58 Y. Li and P. C. Burns, *Can. Mineral.*, 2000, **38**, 727–735.
59 P. C. Burns and K. M. Deely, *Can. Mineral.*, 2002, **40**, 1579–1586.
60 K. T. Lu, Y. Zhang, T. Wei, T. A. Ablott, T. H. Nguyen and R. Zheng, *New J. Chem.*, 2022, **46**, 1371–1380.
61 Y. Zhang, D. J. Fanna, N. D. Shepherd, I. Karatchevtseva, K. Lu, L. Kong and J. R. Price, *RSC Adv.*, 2016, **6**, 75045–75053.
62 N. D. Shepherd, Y. Zhang, I. Karatchevtseva, J. R. Price, L. Kong, N. Scales and G. R. Lumpkin, *Polyhedron*, 2016, **113**, 88–95.

63 E. R. Vance, Y. Zhang and Z. Zhang, *J. Nucl. Mater.*, 2010, **400**(1), 8–14.
64 Y. Zhang, T. Wei, Z. Zhang, L. Kong, P. Dayal and D. J. Gregg, *J. Am. Ceram. Soc.*, 2019, **102**(12), 7699–7709.
65 Y. Zhang, L. Kong, I. Karatchevtseva, R. D. Aughterson, D. J. Gregg and G. Triani, *J. Am. Ceram. Soc.*, 2017, **100**(9), 4341–4351.
66 Y. Zhang, L. Kong, R. D. Aughterson, I. Karatchevtseva and R. Zheng, *J. Am. Ceram. Soc.*, 2017, **100**(11), 5335–5346.
67 K. T. Lu, Y. Zhang, T. Wei, Z. Zhang, M. Avdeev and R. Zheng, *J. Eur. Ceram. Soc.*, 2021, **41**, 6000–6009.
68 P. L. Arnold, J. B. Love and D. Patel, *Coord. Chem. Rev.*, 2009, **253**, 1973–1978.
69 N. Belai, M. Frisch, E. S. Ilton, B. Ravel and C. L. Cahill, *Inorg. Chem.*, 2008, **47**, 10135–10140.
70 R. L. Frost, J. Čejka and M. L. Weier, *J. Raman Spectrosc.*, 2007, **38**(4), 460–466.
71 Y. Zhang, J. Čejka, I. Karatchevseva, M. Qin, L. Kong, K. Short, S. C. Middleburg and G. R. Lumpkin, *J. Nucl. Mater.*, 2014, **446**, 68–72.
72 Y. Zhang, I. Karatchevtseva, M. Qin, S. C. Middleburgh and G. R. Lumpkin, *J. Nucl. Mater.*, 2013, **437**, 149–153.
73 J. R. Bartlett and R. P. Cooney, *J. Mol. Struct.*, 1989, **193**, 295–300.
74 A. J. Locock and P. C. Burns, *Am. Mineral.*, 2003, **88**, 240–244.

